Investigating the near-surface conductance with an integrated EM experiment in Bad Königshofen

Klaus Spitzer[1], Bernhard Fluche[2] and Wolfgang Storz[3]

[1] Institut für Geophysik, TU Bergakademie Freiberg, [2] Comsol AB, Göttingen, [3] HGN Hydrogeologie GmbH, Torgau

1 Introduction

The near-surface conductance is an important physical quantity of the Vertical Gradient Method (VG). With the integrated EM experiment in Bad Königshofen (KHF) we are able to approach this parameter using four very different electric and electromagnetic methods. The dissimilar responses obtained are mainly due to the individual current systems applied and the different scale lengths associated with each method.

The vertical gradient is an induction method using magnetic quantities exclusively. It is closely related to magnetotellurics, however, substituting the vertical gradient of the horizontal variational magnetic field for the telluric field according to Maxwell's first equation (Meyer, 1966). The gradient is determined by synchronously operating a surface ($z = 0$) and a subsurface station at depth $z = d$. In our case, the subsurface station consists of a borehole magnetometer which was developed several years ago by the Institute of Geophysics of the University of Göttingen for the Continental Deep Drilling Program of the Federal Republic of Germany (KTB) (Steveling et al., 1991).

There are only a few publications dealing with VG. Land-based in-situ observations were carried out so far only by Hardam (1974), Babour & Mosnier (1989), Meyer (1986), and Schmucker (1986) using surface equipment within mines and by Spitzer (1993) using the aforementioned Göttingen borehole magnetometer. Experiments exploiting the strong gradient at sea were conducted by, e.g., Law & Greenhouse (1981), Ferguson et al. (1990), and Jegen (1997). Using forward modeling, Haak (1986) carried out investigations with respect to the resolvability of a deep crustal conductor. Jones (1983) proposed a high-resolution, fixed-distance magnetometer set to be operated within boreholes.

VG has several advantages, e.g., being less disturbed by near-surface conductivity inhomogeneities and the reduced anthropogenic high-frequency noise at depth. However, the vertical gradient is hard to determine. Using a borehole magnetometer, the full tensor skin effect transfer function $\underline{\underline{A}}$ could be determined for the first time by Spitzer (1993) in a period range from 10 to 6000 s. Still, that approach was limited by the small gradient encountered (approximately 5 to 10 per cent in amplitude and -5° to -10° in phase) and, subsequently, the poor quality of the estimates. Furthermore, the target area around the KTB location consisted of nearly vertical structures and thin graphitic layers so that the electric field and thus the MT response was extremely distorted and complicated.

The experiment described here provides a significantly better determination of $\underline{\underline{A}}$ and gives the opportunity to carry out methodological investigations, especially with respect to other electromagnetic and electric methods, and to experimentally prove the advantages described above. MT tensor impedances are derived from MT sites that were operated simultaneously during the field survey. They are compared to those derived from VG. The experiment shows that MT and VG responses agree in terms of the MT tensor and

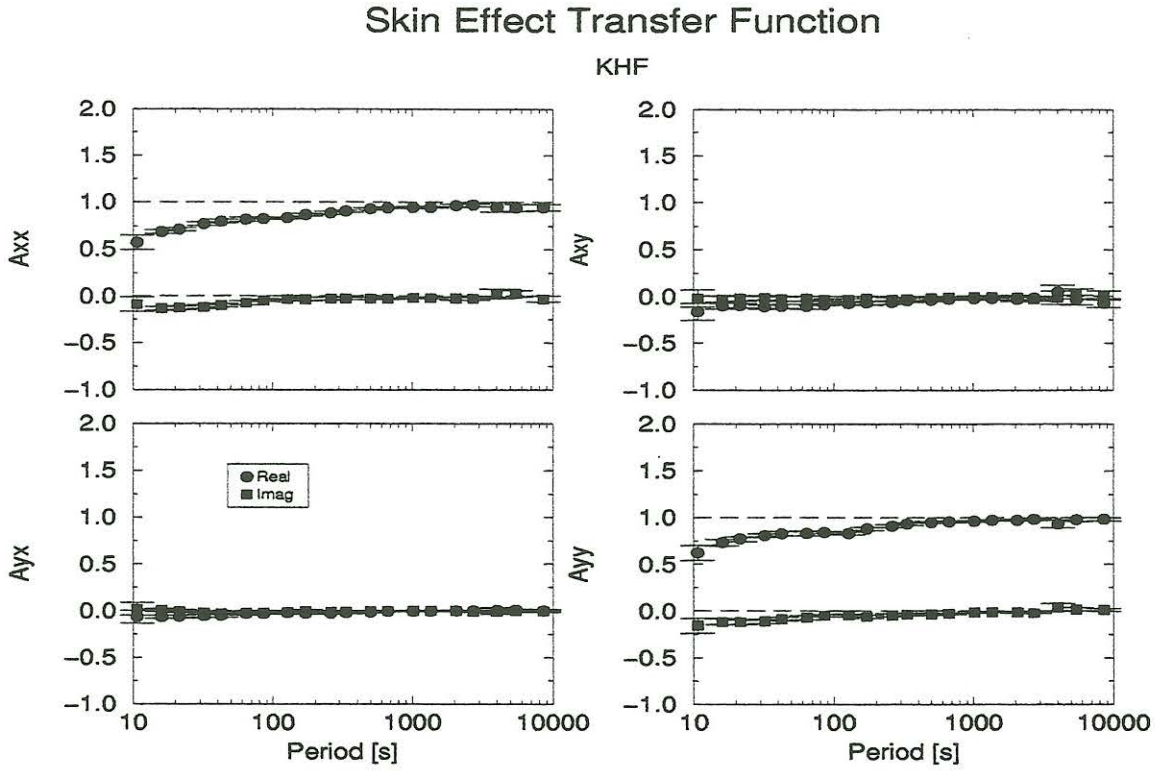

Figure 1: Skin effect transfer function $\underline{\underline{A}}$ for site KHF.

the skin effect transfer function and that the surface electric currents are representative down to a depth of 1 km. In addition, the near-surface structures are investigated using large-scale DC and electric borehole equipment to describe the conductivity distribution between the surface station and the borehole magnetometer. As a matter of fact the rather straightforward environment at KHF provides a favorable study area.

2 The skin effect transfer function

The full skin effect transfer function matrix $\underline{\underline{A}}(\omega)$ represents the bivariate relationship between the variational horizontal magnetic fields downhole and at the surface as a function of angular frequency ω

$$\boldsymbol{B}^d(\omega) = \underline{\underline{A}}(\omega)\boldsymbol{B}^0(\omega) + \delta\boldsymbol{B}^d(\omega) \quad , \tag{1}$$

where $\delta\boldsymbol{B}^d$ denotes uncorrelated noise assumed to be in the downhole magnetic component $\boldsymbol{B}^d$. The elements of $\underline{\underline{A}}$ are estimated by standard least–squares minimization of the error terms. Spectral estimates are obtained by smoothing raw spectral values with a Parzen–window and by stacking a number of intervals. The statistical errors are calculated by a standard method and refer to a probability of 68%. The harmonic coefficients have been determined in a period range from 10 to 8600 s using the robust statistical method of Junge (1993). Fig. 1 shows $\underline{\underline{A}}$ for site KHF. A significant skin effect of approximately 30% in amplitude and -10° in phase is visible at the short period end. Note the relatively small errors and the smoothness of the functions.

Let $\underline{\underline{I}}$ be the identity matrix, $\underline{\underline{D}} = \begin{pmatrix} 0 & 1 \\ -1 & 0 \end{pmatrix}$, μ_0 the induction constant, and τ the

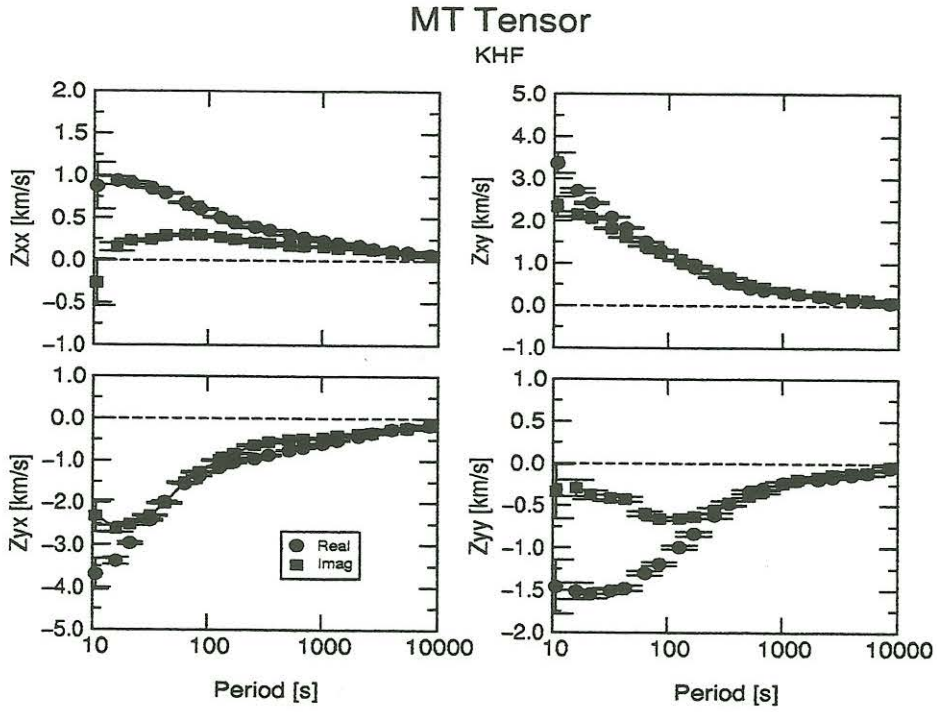

Figure 2: MT tensor $\underline{\underline{Z}}^{MT}$ for site KHF.

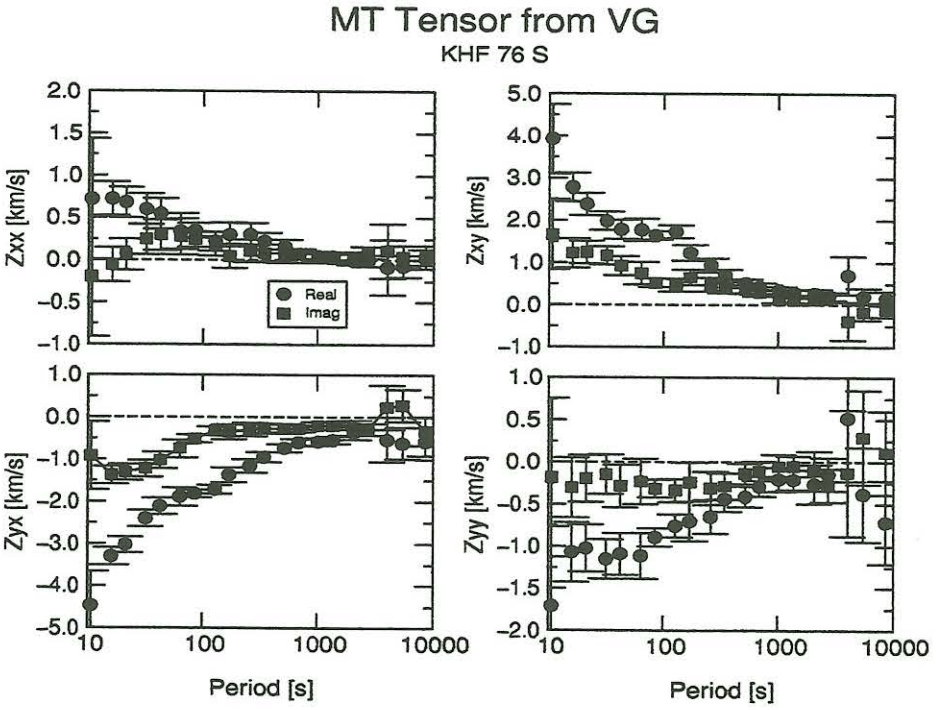

Figure 3: MT tensor $\underline{\underline{Z}}^{VG}$ derived from VG for site KHF.

depth-integrated conductance between the surface and the depth d. Then an approximative relation between skin effect transfer function $\underline{\underline{A}}$ and the MT tensor $\underline{\underline{Z}}^{VG}$ reads

$$\underline{\underline{Z}}^{VG} = \underline{\underline{D}}(\underline{\underline{I}} - \underline{\underline{A}})/\mu_0\tau \ , \tag{2}$$

if the magnetic field is sufficiently homogeneous in the horizontal directions. In our case the relation between the horizontal magnetic components and $\partial B_z/\partial x$ or $\partial B_z/\partial y$, respectively, are in the order of magnitude of 0.001 km^{-1} in the period range from 10 to 1000 s whereas the partial derivatives of B_x and B_y with respect to z are at least 0.1 km^{-1}. For periods above 1000 s the latter do converge toward zero, however, the spatial variations of B_z vanish almost completely.

MT sites that were operated in parallel provide the classical MT tensor

$$\boldsymbol{E}(\omega) = \underline{\underline{Z}}^{MT}(\omega)\boldsymbol{B}^0(\omega) + \delta\boldsymbol{E}(\omega) \tag{3}$$

in the same frequency range as the skin effect transfer function so that a comparison between both responses becomes possible. The MT response $\underline{\underline{Z}}^{MT}$ is shown for site KHF in Fig. 2. Fig. 3 shows the MT tensor $\underline{\underline{Z}}^{VG}$ derived from VG according to eq. (2). Note the excellent agreement of both approaches. This experiment verifies the MT tensor in all details by measuring the magnetic skin effect in a period range from 10 to 1000 s, i.e., the electric fields measured at the surface are representative down to a depth of 1000 m.

An even better demonstration of the good agreement is given by the skin effect transfer functions $\underline{\underline{A}}$ derived from MT and VG (Fig. 4). Note the good fit even in some details (e.g., the slight reincrease at the short-period end of the imaginary part of A_{xx}). The chosen conductance is the best-fit conductance $\tau_{bf} = 76$ S, which has been obtained through least-squares optimization.

Fig. 5 shows the complex conductance τ as a function of period. It is derived from VG and MT according to eq. (2) and reads explicitly

$$\tau_{xy} = \frac{1 - A_{yy}}{\mu_0 Z_{xy}} \qquad \text{and} \qquad \tau_{yx} = \frac{A_{xx} - 1}{\mu_0 Z_{yx}} \ , \tag{4}$$

respectively. The real part of τ is relatively constant and positive. However, the imaginary part is not zero as it is supposed to be. The negative values of τ cause a shift to smaller phase angles. It is still not clear what causes this deviation. The absolute average of τ is approximately 76 S, which has been obtained by least-squares optimization as well.

Fig. 6 shows the distortion matrix $\underline{\underline{V}} = \underline{\underline{Z}}^{VG}(\underline{\underline{Z}}^{MT})^{-1}$. The off-diagonals are small and constant. Real parts of the main diagonals are constant as well and approximately 1 which suggests a rather undisturbed environment at KHF. Only the imaginary parts differ from zero significantly which in turn causes the imaginary parts of the complex conductance to be non-zero (Fig. 5). In general, these results show that the local distortion of the telluric field is low which agrees with results derived from surface DC investigations (Spitzer, in press).

A critical point is the determination of the conductance τ, which will be of major interest in the following. As mentioned before, τ is calculated as a least-squares minimization between $\underline{\underline{Z}}^{VG}$ and $\underline{\underline{Z}}^{MT}$ giving a value of $\tau = 76$ S. Now τ will be derived from large-scale DC measurements and from electrical borehole data in addition. Both values appear to be significantly smaller than the one derived from VG. We will therefore discuss the physics in each case with respect to the individual spatial scale lengths.

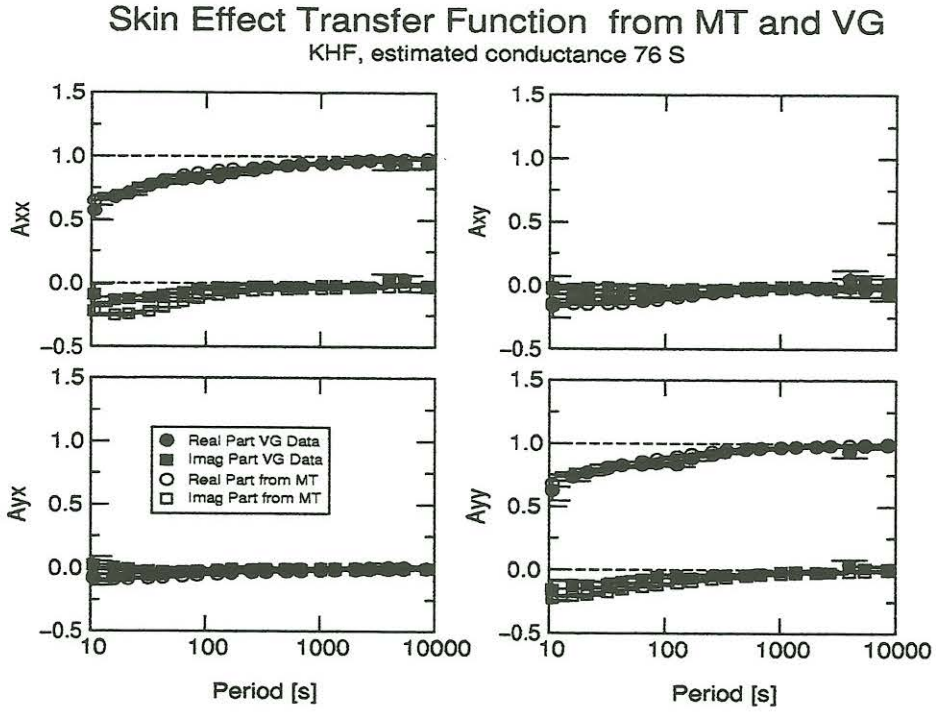

Figure 4: Skin effect transfer functions from MT and VG.

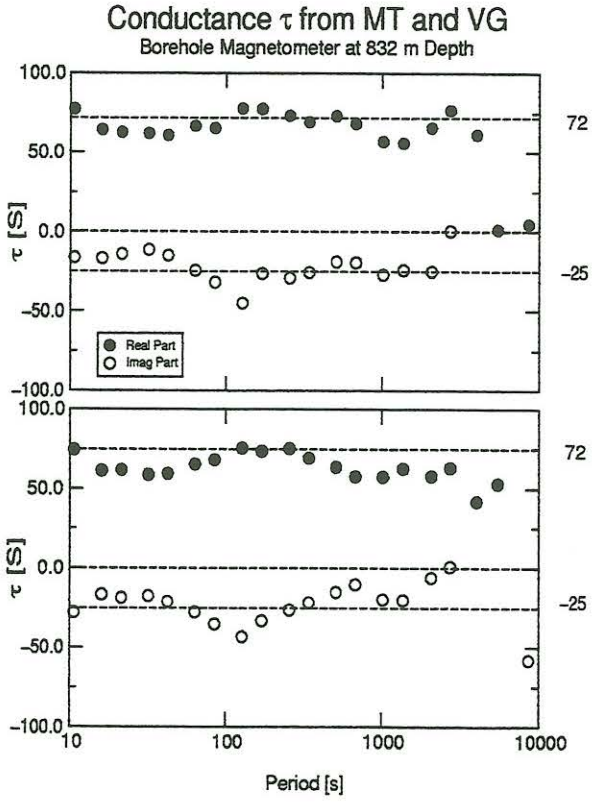

Figure 5: Conductance τ calculated from $\underline{\underline{Z}}^{VG}$ and $\underline{\underline{Z}}^{MT}$.

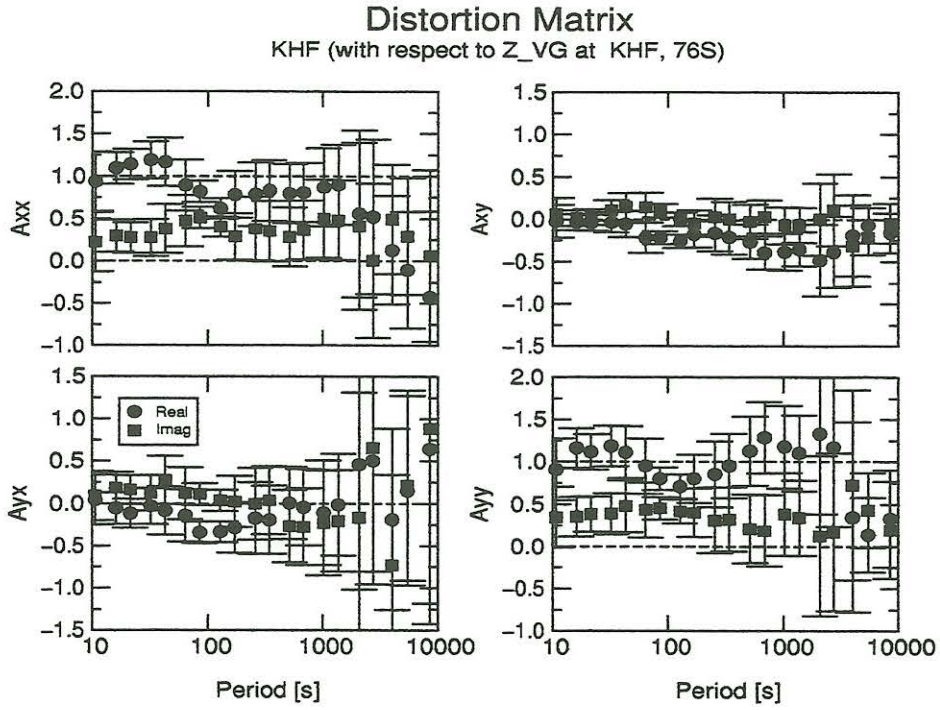

Figure 6: Distortion matrix $\underline{\underline{V}}$ for site KHF.

3 The integrated conductance derived from large-scale DC soundings

The integrated conductance is derived from the layered section of a 3D DC resistivity model (Fig. 7) that has been derived from perpendicularly crossed Schlumberger half-spread soundings. Maximum electrode spacings were 5 km. The model was found through forward modeling. For further details refer to Spitzer (in press). The depth-integrated conductance is determined according to Table 1 and totals approximately 24 S which corresponds to one third of the value derived from VG.

ρ [Ωm]	z [m]	τ [S]
30	0 – 32	1.1
100	32 – 42	0.1
30	42 – 90	1.6
1000	90 – 200	0.1
30	200 – 832	21
		$\approx$ 24

Table 1: Determination of the DC integrated conductance according to the model in Fig. 7.

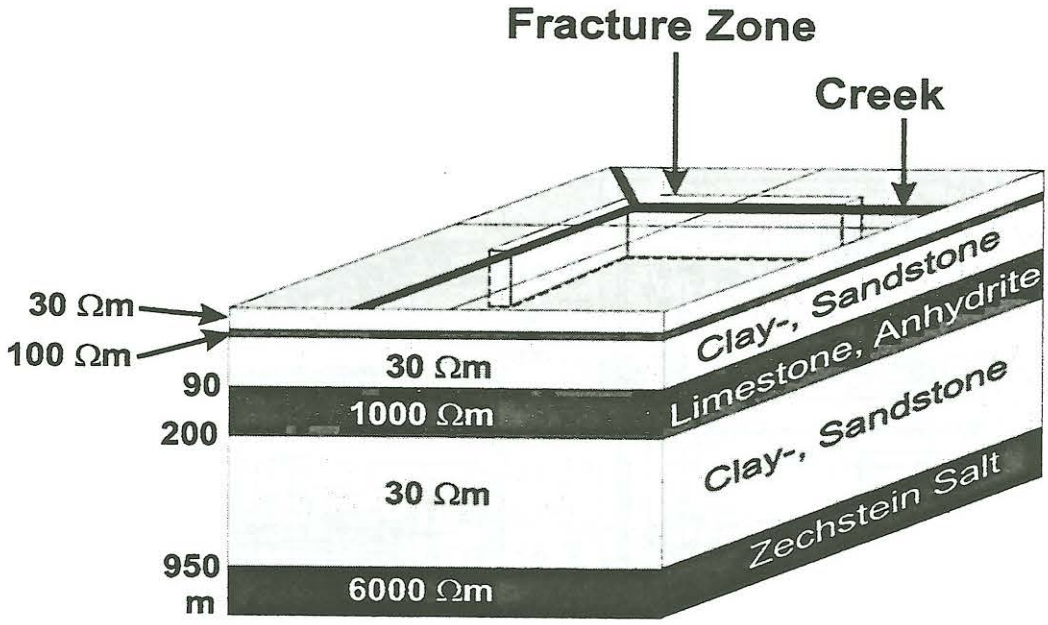

Figure 7: DC resistivity model derived from crossed Schlumberger halfspread soundings at KHF.

4 The integrated conductance derived from electric borehole data

Another approach to determine the conductance uses electric borehole data. The mud in borehole KHF was extremely saline and, thus, highly conductive ($\rho < 0.1$ Ωm) leading to a significant underestimation of the resistivity of the rock matrix. Therefore, the electric borehole logs ES16 (i.e. 16 inches electrode spacing, cf. Fig. 8) and ES64 (i.e. 64 inches electrode spacing) have to be corrected. This is very often done using master curves (Repsold and Mundry, 1990). Here we show as a simple example, how 3D forward modeling can feasibly lead to realistic approximations of the correction factors. More complicated borehole environments including infiltration zones and layering are easily incorporated. As a first approach, the model is restricted to a conductive borehole of 0.2 m in diameter and of 0.1 Ωm resistivity within a homogeneous background of 100 Ωm (Fig. 9). The obtained apparent resistivity logs (left-hand subplot of Fig. 9) thus show lowered values of 25 Ωm and 78 Ωm for ES 16 and ES 64, respectively, at a depth that is supposed to be undisturbed from the surface and the bottom of the borehole. These values yield correction factors of $f_{\text{corr}} = 4$ for ES 16 and $f_{\text{corr}} \approx 1.25$ for ES64. Fig. 10 shows that the corrected logs ES16 and ES64 already agree well after the correction has been applied. The deviation varies within a range of only -10% to 15% over the whole depth range.

FEL (Focussed Electrolog) data were obtained in the borehole as well. Storz (1997) (Fig. 4.19) has applied a correction factor of 2.2 to these data according to an approximation scheme by Repsold (1981). The result agrees well with the corrected ES16/64 data presented here.

The corrected ES16/64-logs are now integrated over the depth from the end of the casing ($\approx$ 450 m) to the magnetometer depth (832 m) giving a conductance of approximately 20 S for ES 16 and 19 S for ES64. If we assume that the conditions are similar

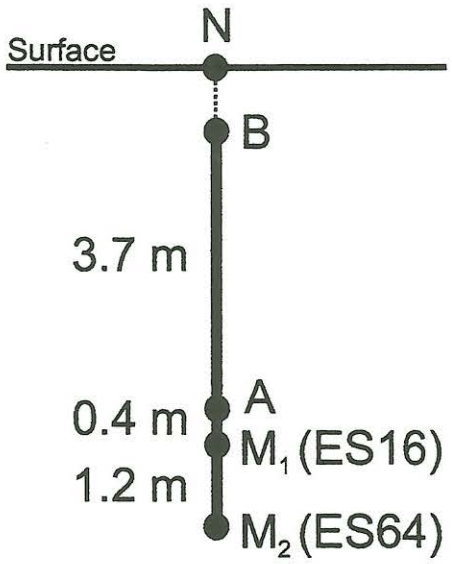

Figure 8: Electrode spacing for electric borehole logs ES16 and ES64.

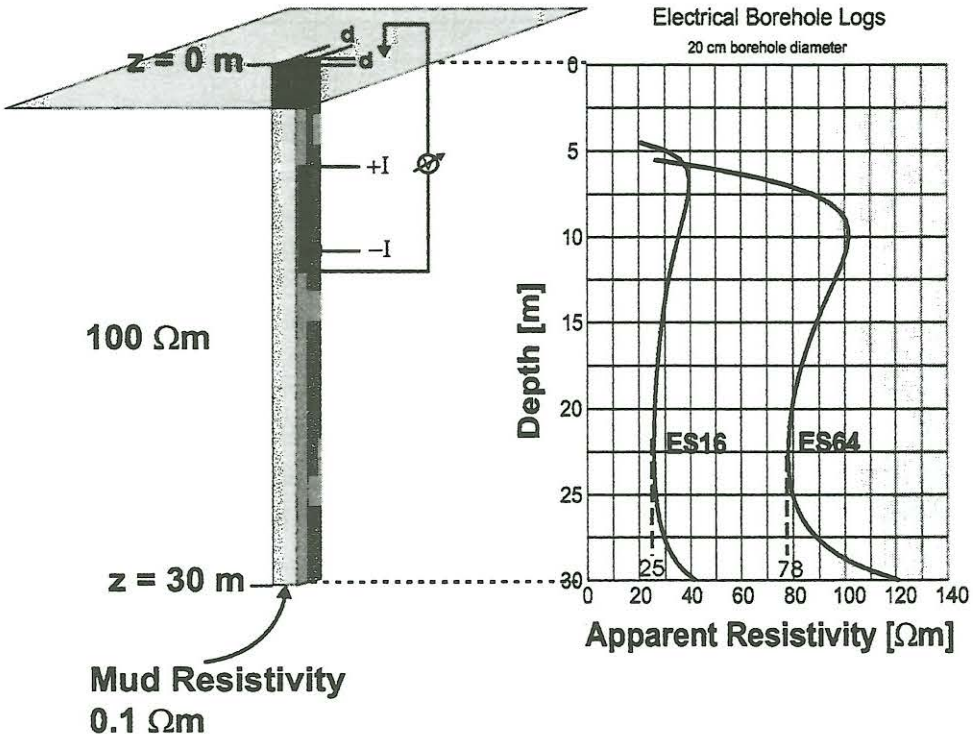

Figure 9: Determination of the correction factors for the electric borehole logs ES16 and ES64. The left-hand subplot shows the simplified model of the borehole. The electrode configuration is according to Fig. 8. The right-hand subplot shows the corresponding synthetic apparent resistivity logs ES16 and ES64 for the model depicted at the left.

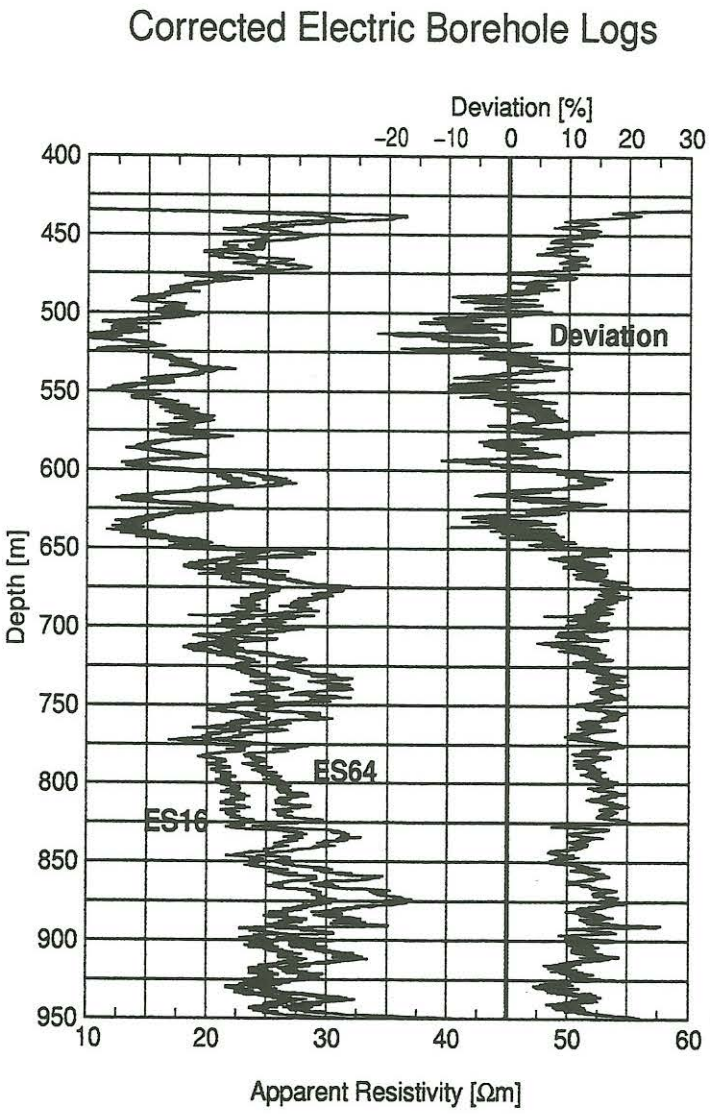

Figure 10: Corrected electric borehole logs ES16 and ES64 and deviation between them.

within the first 450 m, we gain a total conductance of approximately 42 S. Again, this value is only half of the one derived from VG.

5 Discussion

Each of the three methods gives a different value for the depth-integrated conductance τ. VG gives the highest value of 76 S (i.e., an average of approximately 10 Ωm for the first 832 m), borehole resistivity measurements 42 S (i.e. an average of 20 Ωm), and DC the lowest one with 24 S (i.e., 35 Ωm in average). It appears reasonable that the influence of the saline borehole mud is not sufficiently taken into account. Invasion zones would certainly correct the resistivities towards higher values. Furthermore, the borehole mud is more conductive in reality than in the modeled case (0.03 Ωm vs. 0.1 Ωm) which again leads to larger correction factors. This would point to the DC value to be the more

realistic one. It also agrees better with the apparent resistivity values derived from the high-frequency end of mid-band AMT observations at site GAM, 6 km away from KHF (roughly 30 Ωm at 10 Hz, skin depth of approximately 900 m, Bahr et al. (2000)).

On the other hand, both DC methods are associated with non-zero vertical current densitites. This means that a classical small-scale vertical anisotropy (i.e., scale lengths below the electrode spacing of ES 16/64) could cause an unnoticeable shift to lower resistivity values.

Still the value from VG is approximately two to three times higher. Can this be realistic? We know from DC forward modeling and from groundwater mapping that the target area is crisscrossed with conductive fracture zones. These zones did neither influence the borehole measurements nor did they count for calculating the DC conductance. However, they influence the behavior of a large-scale planar magnetic field penetrating into a conductive crust. Consequently, the skin effect must inevitably increase in the presence of the conductive zones. In the following, we outline a way to possibly determine the increase of the skin effect quantitatively. VG sensitivities, which can be calculated numerically, act as weighting factors in the integration. The 1D integrated conductance

$$\tau = \frac{\sum_{i=1}^{N} \phi_i^{VG} \sigma_i}{\sum_{i=1}^{N} \phi_i^{VG}} \, d \quad , \tag{5}$$

is thus adopted to a 3D environment. ϕ_i^{VG} are the VG sensitivities and σ_i the conductivities assigned to the set of grid cells $i = 1, ..., N$ that cover the range from the surface to the magnetometer depth d. In this way we obtain a modified conductance that takes into account lateral conductivity contrasts with respect to their locations and their impact on the skin effect. In our case this should lead to a higher conductance which is required by the observation.

6 Acknowledgments

The authors would like to thank all colleagues who were involved in this project. In particular, we are grateful to Andreas Junge, Uni Frankfurt, who provided us with his robust MT processing code, Erich Steveling, Uni Göttingen, and Thomas Wonik, GGA Hannover, for their activities during the field surveys, and Rüdiger Schulz, GGA Hannover, for his general support. Thanks to Ulrich Schmucker, Göttingen, for many instructive discussions. The project was funded by the Deutsche Forschungsgemeinschaft (Schu 684/2-1).

7 References

Babour, K., and Mosnier, J., 1989, Direct determination of the characteristics of the currents responsible for the geomagnetic anomaly of the Rhinegraben: Geophys. J. R. astr. Soc., **60**, 327–331.

Bahr, K., Bantin, M., Jantos, C., Schneider, E., and Storz, W., 2000, Electrical anisotropy from electromagnetic array data: implications for the conduction mechanism and for distortion at long periods: Phys. Earth Planet. Int., **119**, 237–257.

Ferguson, I., Lilley, F., and Filloux, J., 1990, Geomagnetic induction in the Tasman Sea and electrical conductivity structure beneath the Tasman Seafloor: Geophys. J. Int., **102**, 299–312.

Haak, V., 1986, Ein vertikales magnetotellurisches Profil: Geophysikalische Schlüsselexperimente in der KTB, Forschungskollegium Physik des Erdkörpers, Bochum, 54–59.

Hardam, W., 1974, Direkter Nachweis des Skineffektes anhand von Aufzeichnungen erdmagnetischer Pulsationen über und unter Tage: Diploma thesis, Inst. of Geophysics, Univ. of Göttingen.

Jegen, M., 1997, Electrical properties of the mantle upwelling zone beneath a mid-ocean ridge: An application of vertical gradient sounding: Ph.D. thesis, University of Toronto.

Jones, A., 1983, A passive natural–source twin–purpose borehole technique: Vertical Gradient Magnetometry (VGM): J. Geomag. Geoelectr., **35**, 473–490.

Junge, A., 1993, Induzierte erdelektrische Felder – neue Beobachtungen in Norddeutschland und im Bramwald: Habilitation thesis, Fachbereich Physik, Univ. of Göttingen.

Law, L., and Greenhouse, J., 1981, Geomagnetic variation sounding of the asthenosphere beneath the Juan de Fuca Ridge: J. Geophys. Res., **86**, 967 – 978.

Meyer, J., 1966, Die magneto–tellurische Tiefensondierung und ihr erdmagnetisches Analogon: Gerl. Beitr., **75**, 284–300.

Meyer, R., 1986, Direkter Nachweis des Skineffekts: Diploma thesis, Inst. of Geophysics, Univ. of Göttingen.

Repsold, H., and Mundry, E., 1990, Widerstandsabweichungskurven für Mehrpunktwiderstandsverfahren in Bohrlöchern: Schweizerbart'sche Verlagsbuchhandlung, Stuttgart.

Repsold, H., 1981, Ein systematisches Konzept zur Auswertung von Bohrlochmessungen in Lockergesteinsaquiferen (Aquifere mit intergranularer Porosität): Report No. 87308, NLfB, Hannover.

Schmucker, U., 1986, Erfahrungen mit magnetischen Untertageregistrierungen: Proceedings "Kolloquium Elektromagnetische Tiefenforschung", Deutsche Geophysikalische Gesellschaft, 63–73.

Spitzer, K., 1993, Observations of geomagnetic pulsations and variations with a new borehole magnetometer down to 3000 m depth: Geophys. J. Int., **115**, 839–848.

Spitzer, K., in press, MT static shift and DC sensitivity: Geophys. J. Int.

Steveling, E., Spitzer, K., and Leven, M., 1991, Vertical gradient of horizontal geomagnetic variations — first results with the Göttingen borehole magnetometer in the KTB–VB pilot borehole: Scientific Drilling, **2**, 180–187.

Storz, W., 1997, Die vertikalgradientenmethode in kombination mit magnetotellurischen, bohrlochgeophysikalischen und gleichstromgeoelektrischen verfahren zur widerstandsbestimmung in der oberen kruste: Zwischenbericht zum DFG-Vorhaben Schu-684/2-1, Report No. 87308, NLfB-GGA, Hannover.